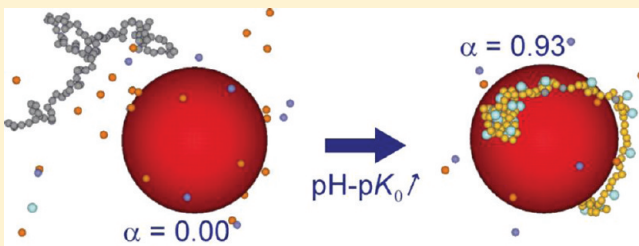


# Adsorption of Weak Polyelectrolytes on Charged Nanoparticles. Impact of Salt Valency, pH, and Nanoparticle Charge Density. Monte Carlo Simulations

Fabrice Carnal and Serge Stoll\*

F.-A. Forel Institute Group of Environmental Physical Chemistry, University of Geneva, 10 Route de Suisse, 1290 Versoix, Switzerland

**ABSTRACT:** Complex formation between a weak flexible polyelectrolyte chain and one positively charged nanoparticle in presence of explicit counterions and salt particles is investigated using Monte Carlo simulations. The influence of parameters such as the nanoparticle surface charge density, salt valency, and solution property such as the pH on the chain protonation/deprotonation process and monomer adsorption at the nanoparticle surface are systematically investigated. It is shown that the nanoparticle presence significantly modifies chain acid/base and polyelectrolyte conformational properties. The importance of the attractive electrostatic interactions between the chain and the nanoparticle clearly promotes the chain deprotonation leading, at high pH and nanoparticle charge density, to fully wrapped polyelectrolyte at the nanoparticle surface. When the nanoparticle bare charge is overcompensated by the polyelectrolyte charges, counterions and salt particles condense at the surface of the polyelectrolyte–nanoparticle complex to compensate for the excess of charges providing from the adsorbed polyelectrolyte chain. It is also shown that the complex formation is significantly affected by the salt valency. Indeed, with the presence of trivalent salt cations, competition is observed between the nanoparticle and the trivalent cations. As a result, the amount of adsorbed monomers is less important than in the monovalent and divalent case and chain conformations are different due to the collapse of polyelectrolyte segments around trivalent cations out of the nanoparticle adsorption layer.



## 1. INTRODUCTION

Polyelectrolytes have constituted an important research field<sup>1–6</sup> for several years due to their large involvement in essential industrial (bio, pharma, food, fragrances, and flavors) and natural processes.<sup>7–11</sup> Long-range intra- and intermolecular Coulomb electrostatic interactions arising from charged polyelectrolyte monomers lead to particular physicochemical properties and adsorption behavior in the presence of oppositely charged substrates such as polyelectrolytes,<sup>12</sup> dendrimers,<sup>13</sup> nanoparticles,<sup>9</sup> flat surfaces,<sup>14</sup> or biomacromolecules.<sup>15</sup> Additional length scales are introduced to the system complexity<sup>16</sup> and the control of parameters influencing the polyelectrolyte solution and interface behavior remains not fully understood and, thus, represents a great challenge. In addition, small charged mobile counterions and salt particles strongly interact with polyelectrolytes and charged substrates thus modifying the subtle competition between attractive and repulsive electrostatic interactions.

The pH influence on acid/base properties of weak polyelectrolyte chains was significantly studied experimentally and theoretically by determining potentiometric titration curves.<sup>17</sup> Empirical theories were proposed to link together experimental parameters such as pH, degree of ionization  $\alpha$ , and  $pK$ . It is well-known that the titration of isolated monoprotic acids can be described by the Henderson–Hasselbalch equation, and the corresponding  $pK_a$  values are easily identifiable. In real systems, the  $pK_a$  determination is more complicated due to electrostatic

interactions between charged polyprotic titration sites.<sup>18,19</sup> The titration of monoprotic polyelectrolyte chains gives the usual curves, i.e., the increase of  $\alpha$  with pH, and a shift with the isolated monomer curve is obtained.<sup>20</sup> For coupling strengths greater than those corresponding to aqueous polyelectrolytes, nonmonotonic behavior of the degree of ionization in function of the pH solution was observed.<sup>21</sup>

The complexation between polyelectrolytes and charged macroions was experimentally studied by Dubin and co-workers to better understand binding processes. Different charged substrates and charge distributions were investigated such as micelles,<sup>22</sup> dendrimers<sup>23</sup> or globular proteins.<sup>3</sup> McQuigg et al.<sup>24</sup> showed that the adsorption/desorption limit was proportional to the inverse Debye screening length confirming the importance of ionic strength in the complex formation process. Using the electrostatic self-assembled and charge compensation properties between polyelectrolytes and ionic surfactant micelles, stable “supermicellar” aggregates exhibiting core–shell microstructures were formed opening the way to new biomedical applications.<sup>9,25</sup> Unstable inorganic oxide nanoparticles such as cerium oxides were also stabilized with polyelectrolytes over a large range of pH, ionic strength, and concentration by the irreversible coating

**Received:** June 15, 2011

**Revised:** August 19, 2011

**Published:** September 08, 2011

with short poly(acrylic acid) chains.<sup>26</sup> The mixing concentration is of main importance in the formation of electrostatic self-assembled colloidal complexes between surfactants and polyelectrolytes since the complex structure, which is spherical at low concentration, may undergo a sphere-to-cylinder transition with the increase of concentration.<sup>27</sup> The mixing ratio influence was also observed by Wang and Roman<sup>11</sup> during the complex formation between chitosan and cellulose nanocrystal. The authors obtained spherical particles with higher chitosan concentrations and nonspherical complexes at lower chitosan ratio. Recently, Koupanou et al.<sup>28</sup> showed that the stabilization efficiency of lead sulfide nanoparticles by cationic polyelectrolytes depends on the primary structures of the chains and is not directly controlled by the electrostatic.

The issue of electrostatic interactions between charged objects and more particularly polyelectrolytes and macroions has also been studied theoretically and by computer simulations leading to several reviews.<sup>4–6,29,30</sup> Theoretical phase diagrams of the complexation of semiflexible polyelectrolytes with oppositely charged macroions reveal that complexes with fully wrapped chains are obtained at intermediate salt concentration and high macroion charge. Moreover, two dewrapping transitions occur at very low and very high salt concentrations.<sup>31,32</sup> Particular complex conformations such as rosette structures were analytically predicted with scaling theories in which the chain stiffness was shown to be the most important.<sup>33,34</sup> Indeed, polyelectrolyte wrapped to rosette transition occurs with an increase of the persistence length. For a given chain persistence length, Manning<sup>35</sup> demonstrated that the stability limits of complexes between polyelectrolytes and charged curved surfaces was imposed by the surface curvature resulting in a more difficult chain adsorption process to smaller macroions. Analytical expressions for critical radius and surface charge density to observe chain adsorption were also provided by Winkler and Cherstvy.<sup>36</sup> Due to correlation effects, the charge inversion of the charged spherical particles was found to occur if the total polyelectrolyte charge is larger than particle charges.<sup>37</sup> Comparing with neutral polymer chains, it was shown by extended mean-field theory that an extra degree of freedom is introduced by the presence of the counterions of weakly charged polyelectrolytes hence improving the miscibility between the chains and polar nanoparticles.<sup>38</sup>

The influence of various physicochemical parameters on the complexation between polyelectrolytes and oppositely charged macroions was also studied by computer simulations during the last years. It was shown that chain stiffness significantly influences the complexation of strong polyelectrolytes and conformational structures such as rosette, solenoid, and tennis ball were observed depending on ionic strength, chain length, and rigidity.<sup>39–42</sup> The chain length and macroion size were also found to be the most important since a stronger adsorption process is shown if the chain length to macroion diameter ratio is low.<sup>43,44</sup> Carlsson et al.<sup>45</sup> performed Monte Carlo simulations with an inhomogeneous charge distribution at the macroion surface and found a higher number of adsorbed chain monomers in comparison with the homogeneous charge distribution. The charge regulation at the macroion surface makes the complexation of polyelectrolyte chains with proteins possible even when the solution pH is at the protein isoelectric point thus compensating for the Coulombic charge–charge interactions.<sup>46</sup>

The adsorption of a polyelectrolyte chain at the surface of a spherical particle showed a nonmonotonic behavior of the chain radius of gyration with an increase in the salt concentration.

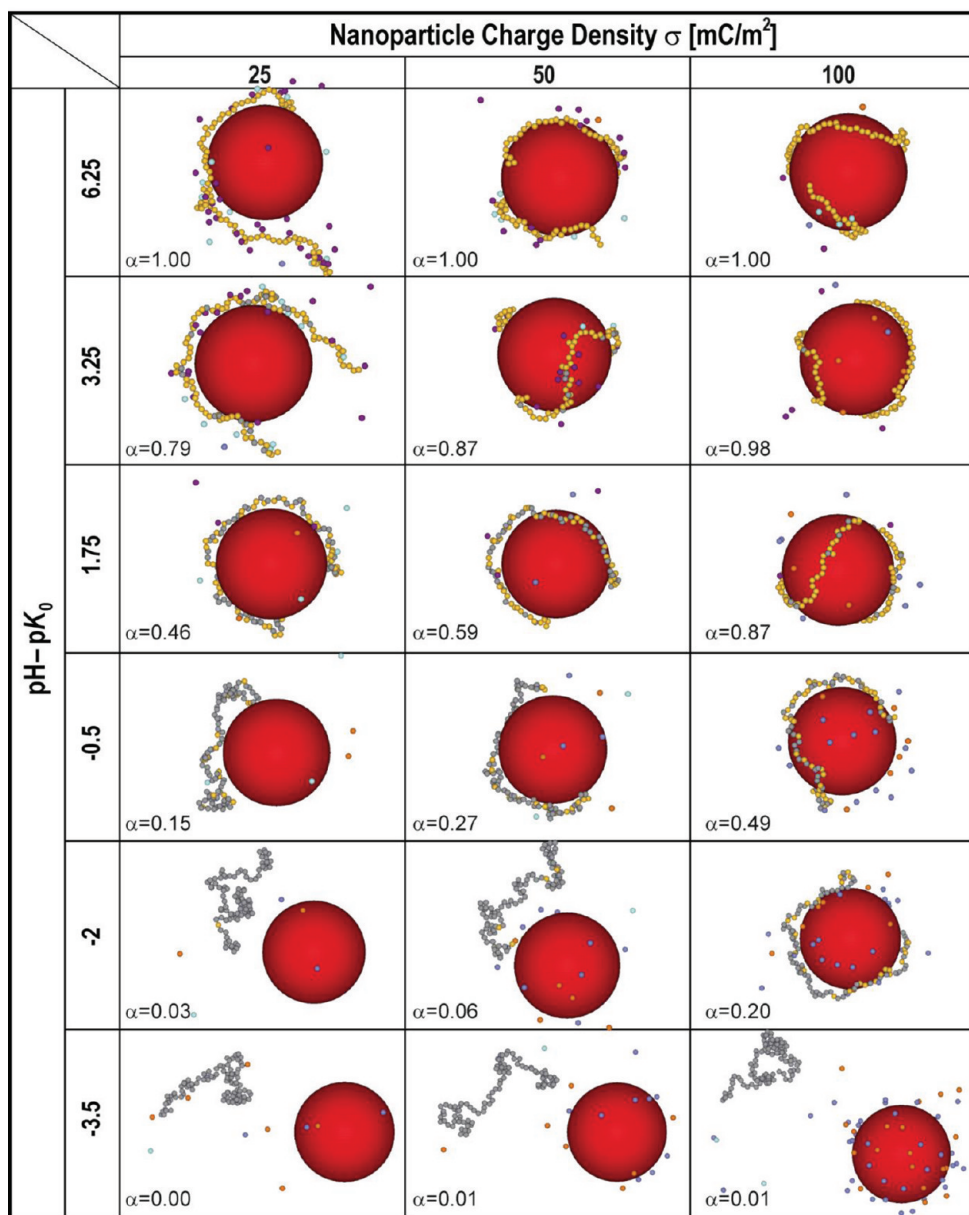
Adsorbed and desorbed states were identified due to significant fluctuations of the chain radius of gyration with the increase of the ionic strength. The transition between the two states was found to be sharp like a first-order phase transition.<sup>44,47</sup> To get practical information for the rational synthesis of stabilizers and destabilizers of colloidal particles, Hu et al.<sup>48</sup> investigated by Brownian dynamics the mechanism of a two-head polyelectrolyte chain affecting the static and dynamic behavior of spherical macroions.

The issue of conformational behavior and pH variations was extensively studied from an analytical point of view by Ullmer and co-workers<sup>49,50</sup> by computer simulations using screened Coulomb potentials and explicit simple ions. Monte Carlo simulations were also used to gain insight into the conformational behavior of poly(acrylic acid) chains as a function of pH.<sup>51</sup> To address the nanoparticle–polyelectrolyte issue, we investigated in a systematic way the influence of pH in the complexation process of weak polyelectrolyte chains with oppositely charged nanoparticles.<sup>52,53</sup> Debye–Hückel potentials with monovalent salt were considered and phase diagrams were obtained by considering different nanoparticle sizes and surface charges, ionic strengths, polyelectrolyte contour lengths, and intrinsic rigidities. Multivalent ions, which are naturally occurring, are known to induce drastic conformational changes of polyelectrolyte chains or dendrimers<sup>54–57</sup> via local specific interactions with the polyelectrolyte chains. Such effects observed with multivalent ions might not have been explained by Debye–Hückel approximations. In this paper, we perform Monte Carlo simulations with full Coulomb electrostatic potential to gain insight into the influence of explicit multivalent salt particles and pH in the complexation process of weak polyelectrolyte chains on spherical nanoparticles. Strong local correlations as well as competitions between charged monomers, nanoparticle surface, and explicit multivalent ions are found to modify significantly the polyelectrolyte conformation at the nanoparticle surface with important implications on the understanding of many biological systems (DNA and nucleosome complexes) and for the rational use of polyelectrolyte and nanoparticle based mixtures (gene therapy).

## 2. MODEL

Monte Carlo (MC) simulations are performed at 298 K in the grand canonical ensemble according to the Metropolis algorithm.<sup>58</sup> An off-lattice three-dimensional coarse grained model is used to describe the system and the objects evolve in a periodic cubic box of 400 Å. The solvent, here water, is treated implicitly as a dielectric medium with a relative dielectric permittivity constant  $\epsilon_r = 78.54$  taken as that of water. The nanoparticles (NPs), polyelectrolyte monomers, counterions, and salt particles are described by impenetrable hard spheres to take into account the excluded volume effect. Weak polyelectrolyte chains (PEs) are represented as a succession of 100 freely jointed monomers of radius  $R_m = 2$  Å so that the Manning counterion condensation domain is reached when the chain ionization degree  $\alpha > 0.56$ .<sup>59</sup> The NP and PE counterions as well as salt anions and monovalent salt cations have fixed radii of 2 Å while di and trivalent salt cations radii are equal to 2.5 Å. The NP radius  $R_{NP}$  is set to 35.7 Å and the surface charge density  $\sigma$  [mC/m<sup>2</sup>] is adjusted by the value of the charge located at its center. A constant and homogeneous charge distribution is thus obtained at the nanoparticle surface. Counterions and salt particles have a permanent charge on their center of +1 for PE

**Table 1.** Monte Carlo Simulations of a Weak Flexible PE Chain and One NP Surrounded by Explicit Monovalent Counterions and Monovalent Salt Particles<sup>a</sup>



<sup>a</sup> Neutral and charged monomers are represented by grey and yellow spheres; PE and NP counterions, by purple and blue spheres; and salt particles, by cyan spheres. Cases with NP surface charge densities  $\sigma$  ranging from 25 to 100 [mC/m<sup>2</sup>] are considered. The degree of ionization  $\alpha$  is calculated as a function of  $pH - pK_0$ . Chain deprotonation promotes the monomer adsorption at the NP surface releasing a few NP counterions in bulk. PE counterions and salt cations are attracted by the PE chain only when its linear charge density is higher than the NP bare charge. The increase of  $\sigma$  allows stronger PE–NP interactions hence promoting the PE deprotonation.

counterions,  $-1$  for NP counterions,  $+1$ ,  $+2$ , or  $+3$  for salt cations, and  $-1$  for salt anions. Since the PE linear charge density is pH dependent, each monomer is a titrating site which can be neutral or negatively charged ( $-1$ ). During the whole simulations, salt concentration is fixed to  $1 \times 10^{-3}$  M.

The NP is placed at the center of the box and does not move during the whole MC runs. The NP and PE counterions as well as salt particles are moved through the box by translational movements. The flexible PE chain conformation is modified by well-known specific movements such as kink-jump, end-bond, reptation, and partially clothed pivot. Within the box, all pairs of

charged objects interact with each other via a full Coulomb electrostatic potential which is positive or negative when repulsive or attractive interactions are considered and is defined as

$$U_{ij}(r_{ij}) = \begin{cases} \infty, & r_{ij} < R_i + R_j \\ \frac{z_i z_j e^2}{4\pi\epsilon_0\epsilon_r r_{ij}}, & r_{ij} \geq R_i + R_j \end{cases} \quad (1)$$

where  $e$  is the elementary charge ( $1.6 \times 10^{-19}$  C),  $\epsilon_0$  is the permittivity of the vacuum ( $8.85 \times 10^{-12}$  C V<sup>-1</sup> m<sup>-1</sup>),  $z_{ij}$  is the

charges carried by monomers, the NP, counterions, or salt particles,  $r_{ij}$  is the distance between them (center–center), and  $R_{ij}$  is their radii. Thus the total energy  $E_{\text{tot}}$  for a given conformation which also includes hard core interactions is given by the sum of the whole pairwise potentials  $U_{ij}$ . As the system considered here is very diluted (only one PE and one NP), the electrostatic is calculated without introducing cutoff functions.

During the MC simulations, only the charges of PE chains can vary with pH. Thus the acceptance of each protonation/deprotonation step of the PE monomers is related to the MC Metropolis selection criterion as follows:<sup>60</sup>

$$\Delta E = \Delta E_{\text{tot}} \pm k_B T \ln 10(pH - pK_0) \quad (2)$$

where  $k_B$  is the Boltzmann constant ( $1.3807 \times 10^{-23} \text{ J K}^{-1}$ ) and  $T$  is the temperature (298 K). The second term represents the change of free energy of the intrinsic association reaction of a monomer. The signs minus and plus are used when the monomers are deprotonated and protonated, respectively. After 10 000 MC step cycles to achieve chain relaxation, each N/8 monomer charge is switched on or off depending on whether the monomer is neutral or charged, and oppositely charged counterions are randomly inserted or removed when charges appear or disappear on the chain, respectively, to keep the system electrostatically neutral. The addition of explicit counterions results from the presence of an alkali such as NaOH. During the titration processes, the simulation box is coupled to a proton bath to establish a constant pH. Indeed, in the grand canonical ensemble, the chemical potential (through  $pH - pK_0$  values), the box volume, and the temperature are fixed; only the particle number may vary. For a given  $pH - pK_0$  value, an energy stabilization equilibration period of  $2.5 \times 10^5$  MC steps is achieved then followed by a production period of  $7.5 \times 10^5$  steps where observables such as the chain degree of ionization  $\alpha$ , PE radius of gyration  $\langle R_g^2 \rangle$  as well as the number of monomers in trains  $N_{\text{train}}$ , tails  $N_{\text{tail}}$ , and loops  $N_{\text{loop}}$  or the monomer radial distribution function around the NPs are recorded to calculate mean values.

The titration of isolated monomers in the total absence of electrostatic interactions between them corresponds to an ideal system and allows us to define the dissociation constant of monomers  $K_0$  introduced via the Henderson–Hasselbalch equation

$$pK_0 = pH - \log \left( \frac{\alpha}{1 - \alpha} \right) \quad (3)$$

where  $pK_0$  represents the negative logarithm of the constant. Acid/base properties of PE monomers are different from ideal case due to their connectivity with each other. Thus the apparent dissociation constant  $K$  changes and the difference of acid/base properties of PE monomers and isolated monomers is expressed by

$$\Delta pK = pK - pK_0 = pH - pK_0 - \log \left( \frac{\alpha}{1 - \alpha} \right) \quad (4)$$

Therefore removing a proton from PE chains is more and more difficult when the degree of ionization  $\alpha$  increases leading to the decrease of the apparent dissociation constant  $K$ .<sup>61</sup>

In this study, the thickness of the first layer of monomer adsorption  $\text{Ads}_L$  around NPs is defined as follow:

$$R_{\text{NP}} + R_m \leq \text{Ads}_L \leq R_{\text{NP}} + 3R_m \quad (5)$$

PEs are thus considered adsorbed if at least one monomer center is situated in the  $\text{Ads}_L$  more than 50% of MC steps during the production period. Adsorbed PEs are composed of three parts: (i) trains, continuous monomers lying in  $\text{Ads}_L$ ; (ii) loops, PE segments situated between two trains; and (iii) tails, PE segments which rise up in bulk without returning to the NP first adsorption layer.

### 3. RESULTS AND DISCUSSION

#### 3.1. Complex Formation in Presence of Monovalent Salt.

The case of an isolated weak flexible PE chain and one NP surrounded by explicit monoanionic counterions and monovalent salt particles at  $C_i = 1 \times 10^{-3} \text{ M}$  is first investigated. Chains composed of 100 monomers and NP surface charge densities  $\sigma$  ranging from 25 to 100 [ $\text{mC/m}^2$ ] are considered. Equilibrated conformations are presented in Table 1 for various  $\sigma$  and  $pH - pK_0$  values. In the inset of each cell,  $\alpha$  represents the mean chain degree of ionization. Globally, the PE deprotonation process is improved by the increase of  $pH - pK_0$  values which promotes the adsorption of PE monomers on the NP. During the titration process, several competitive electrostatic interactions occur (PE with NP, PE and NP with salt particles as well as PE and NP with their counterions). The NP effective charge is then modified by the presence of its counterions, salt anions, and PE monomers whereas attractive interactions between monomers and counterions, salt cations, and NP affect the PE linear charge density. As shown in Table 1 by increasing  $pH - pK_0$ , the PE chain progressively “moves” closer to the NP surface releasing a few NP counterions in the bulk. The PE–NP complexation allows equilibrated conformations of low energy to be obtained due to strong monomer–NP attractive interactions. When the PE linear charge density becomes higher than the NP bare charge, PE counterions and salt cations are attracted around the PE chain in order to reduce the system electrostatic energy (Table 1, e.g., when  $\alpha = 1$  and  $\sigma = 25$  and  $50 \text{ [mC/m}^2]$ ). At a given  $pH - pK_0$  value, the increase of  $\sigma$  promotes the PE deprotonation due to an increase of the attractive interactions between monomers and NP. Furthermore, the PE adsorption shows more regular structures at high  $pH-pK_0$  and  $\sigma$  values where an onset of tennis ball conformation is observed (Table 1 at  $\sigma = 100$  and  $\alpha = 1$ ). Comparing with theoretical diagram of states provided by Schiessl,<sup>34</sup> our situations belong to the low ionic strength with a Debye length of 9.67 nm. Since our PE chains are fully flexible (i.e., we do not introduce any intrinsic rigidity bond angle), we do not observe rosette conformations. When PE overcharges the macroion, the appearance of one or two tails was predicted. In our case, this feature can be observed when  $\sigma = 25$  and  $50 \text{ [mC/m}^2]$  with  $\alpha$  values up to 0.25 and 0.50, respectively. The formation of tails is significant at low  $\sigma$  values. It should be noted that tail formation is also observed in cells by considering DNA-histones complexes owing to the charge excess remaining from DNA chains.<sup>62</sup>

**Titration Curves.** Figure 1a represents PE titration curves in presence of NPs with surface charge densities of 25, 50, 75, and 100 [ $\text{mC/m}^2$ ]. For comparison, titration curves for isolated PE chains and monomers are also given. The corresponding  $\Delta pK$  variations are calculated in Figure 1b. It is clearly shown that the presence of one NP plays a significant role by promoting PE deprotonation. On one hand, the titration curve of the isolated chain is always situated above the ideal case due to the connectivity between monomers which makes the deprotonation

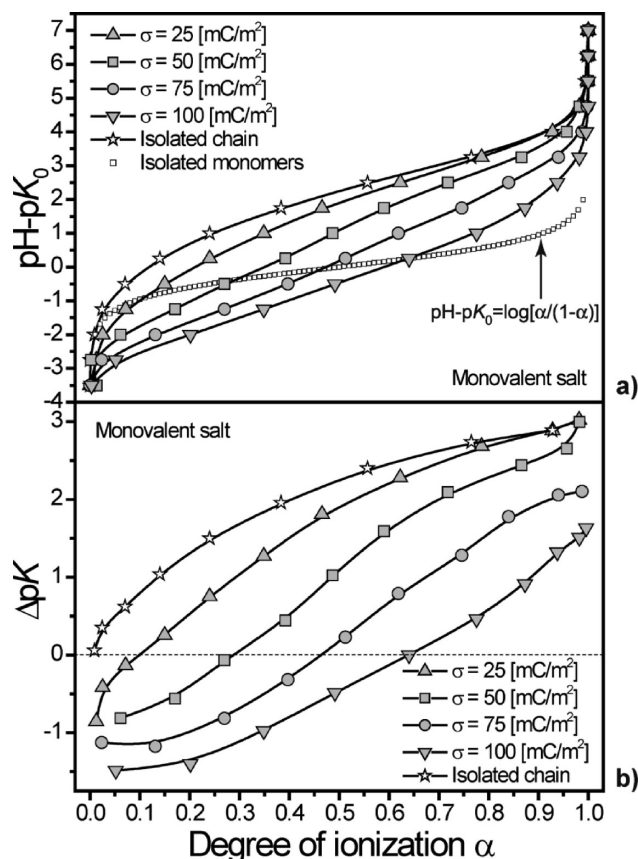


**Figure 1.** (a) Monte Carlo titration curves and (b)  $\Delta\text{p}K$  variations calculated as a function of  $\alpha$  for a weak PE chain in presence of one NP surrounded by monovalent counterions and salt particles. The PE deprotonation is promoted by the NP and higher surface charge densities  $\sigma$  leading to PE titration curves situated below the isolated chain. Due to the increase of PE–NP interactions with  $\alpha$ , titration curves cross the ideal curve for the whole  $\sigma$  values.

process more difficult. On the other hand, titration curves in the presence of one NP show a different behavior since they cross the ideal curve. At the crossing points, the repulsive monomer–monomer interactions are counterbalanced by the attractive monomer–NP ones and  $\Delta\text{p}K = 0$  (Figure 1b). PE degrees of ionization are equal to 0.11, 0.29, 0.47, and 0.64 when the ideal curve is crossed at  $\sigma = 25, 50, 75$ , and  $100 [\text{mC/m}^2]$ , respectively. Indeed, higher NP surface charge densities result in stronger electrostatic interactions with monomers hence counterbalancing higher PE intramolecular electrostatic interactions. Thus for a given  $\text{pH} - \text{p}K_0$  value,  $\alpha$  regularly increases with  $\sigma$  from the isolated curve chain. For all of the  $\sigma$  values considered here,  $\Delta\text{p}K$  values are negative when monomer–NP attractive electrostatic interactions are stronger than repulsive monomer–monomer interactions. Such situations occur when  $\alpha$  values are below 0.11, 0.29, 0.47, and 0.64 for  $\sigma = 25, 50, 75$ , and  $100 [\text{mC/m}^2]$ , respectively. In such a domain, the NP promotes the PE deprotonation process with  $\Delta\text{p}K < 0$ . By increasing further  $\text{pH} - \text{p}K_0$ ,  $\Delta\text{p}K$  values become positive and monomer–monomer electrostatic repulsions are then strong enough to overcompensate PE–NP attractive interactions. Furthermore, we observe that on one hand  $\Delta\text{p}K$  values with  $\sigma = 25$  and  $50 [\text{mC/m}^2]$  are quasi-identical to the isolated chain case when PEs are almost fully charged hence showing that the NP has only a very limited

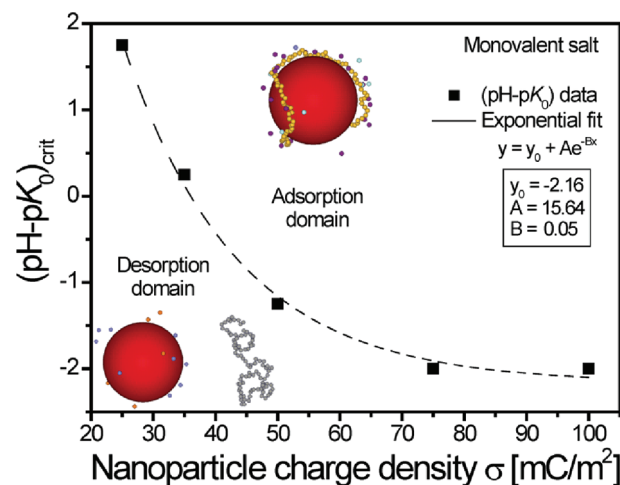


**Figure 2.**  $\text{pH} - \text{p}K_0$  values at which the weak PE chain is desorbed from the NP surface  $(\text{pH} - \text{p}K_0)_{\text{crit}}$  represented as a function of the NP surface charge density  $\sigma$ . Explicit monovalent counterions and salt particles are present. Attractive interactions between the PE and NP increase with  $\sigma$  promoting the monomer adsorption. The adsorption domain is then larger at high NP charge densities.  $(\text{pH} - \text{p}K_0)_{\text{crit}}$  values are following an exponential decay with the increase of  $\sigma$ .

effect on the PE deprotonation process at high  $\alpha$  values. On the other hand, significant differences occur within the whole titration range considering curves at  $\sigma = 75$  or  $100 [\text{mC/m}^2]$  with the isolated chain (Figure 1b) hence confirming the NP influence on the PE titration process even at high chain degree of ionization due to strong electrostatic interactions.

It has to be noted that the titration curves in Figure 1a show usual shapes, i.e., the increase of the chain degree of ionization with  $\text{pH} - \text{p}K_0$ . As suggested by Onufriev et al.,<sup>18</sup> who decomposed complex titration curves into standard components (quasi-sites), we cannot determine the number of titration sites which are implicated if the curves adopt derived Henderson–Hasselbalch forms. The authors showed that titration sites with very different  $\text{p}K_a$  lead to titration curves with unusual shapes. In our case, the  $\text{p}K_a$  of the different titration sites are not strictly identical since the increase of the NP charge density modifies the acid/base properties of each titration sites. However, the difference between them is expected to be limited because of the usual Henderson–Hasselbalch curve shapes which are found here.

**Adsorption/Desorption Limits.** To capture the main features of PEs adsorption,  $(\text{pH} - \text{p}K_0)_{\text{crit}}$  representing  $\text{pH} - \text{p}K_0$  values at which PE chains are desorbed from the NP surface as well as PE mean-square radii of gyration are calculated and presented in Figures 2 and 3, respectively. The prediction of adsorption/desorption domains is of main importance since PEs are largely involved in flocculation processes which are commonly used for instance in wastewater treatment,<sup>7</sup> and prior to the flocculation, PEs must adsorb at the surface of the colloidal fraction. It is shown in Figure 2 that  $(\text{pH} - \text{p}K_0)_{\text{crit}}$  significantly depends on the NP surface charge densities. Indeed, high  $\sigma$  values allow stronger monomer–NP electrostatic interactions promoting the monomer adsorption. The PE degree of ionization, and consequently  $\text{pH} - \text{p}K_0$ , necessary to observe PE adsorption is then found lower with higher  $\sigma$  values. Furthermore, the variation of  $\sigma$  has more influence on the adsorption/desorption domain at low values. From  $\sigma = 25$  to  $50 [\text{mC/m}^2]$ , a rapid decrease of  $(\text{pH} - \text{p}K_0)_{\text{crit}}$  is observed. Then, the slope of the curve is reduced from

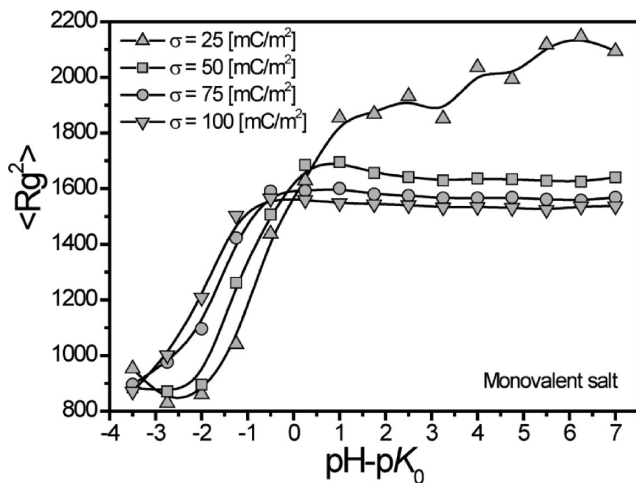


**Figure 3.** Mean square radius of gyration ( $\langle R_g^2 \rangle$ ) versus  $pH - pK_0$  of a PE chain in presence of one NP, monovalent counterions and salt particles. Chain stretching is first observed with the increase of  $pH - pK_0$  leading to the increase of  $\langle R_g^2 \rangle$ . When  $\sigma = 50, 75$ , and  $100$  [ $mC/m^2$ ],  $\langle R_g^2 \rangle$  plateau values are then reached due to chain wrapping around the NP surface and monomer adsorption within the NP first layer. PE chain stretching with  $\alpha$  is then widely limited by the presence of the NP. When  $\sigma = 25$  [ $mC/m^2$ ], PE-NP interactions are not strong enough to adsorb most of monomers in the NP first layer leading to a continuous  $\langle R_g^2 \rangle$  increase with  $pH - pK_0$ .

$\sigma = 50$  to  $75$  and finally, the further increase of  $\sigma$  does not influence  $(pH - pK_0)_{crit}$  anymore since chains are already adsorbed at very low  $pH - pK_0$  values. It has to be noted that the decay of  $(pH - pK_0)_{crit}$  with the increase of  $\sigma$  was found to follow an exponential decay with  $(pH - pK_0)_{crit} \approx e^{-0.05\sigma}$ .

The evolution of PE chain dimensions during the complexation process is now investigated in Figure 3 via the calculation of the PE mean square radius of gyration ( $\langle R_g^2 \rangle$ ). When PEs are fully protonated ( $\alpha = 0$ ), the chains adopt self-avoiding walk (SAW) conformations due to the absence of monomer-monomer as well as monomer-NP electrostatic interactions. The increase of  $pH - pK_0$  first results in a stretching of the chain due to intramolecular repulsive interactions.<sup>63</sup> When PEs are fully adsorbed,  $\langle R_g^2 \rangle$  evolve to plateau values of  $1642$ ,  $1571$ , and  $1537$   $\text{\AA}^2$  for  $\sigma = 50, 75$ , and  $100$  [ $mC/m^2$ ], respectively. These values correspond to the dimensions of the first adsorption layer (upper and lower limits equal to  $1739$  and  $1421$   $\text{\AA}^2$ ) considering the adsorption criterion used in this paper (see Section II). PE chains are long enough to wrap around the whole NP surface and to adopt tennis ball like conformations. It has to be noted that  $(pH - pK_0)_{crit}$  values for  $\sigma = 50, 75$ , and  $100$  [ $mC/m^2$ ] are  $-1.25, -2$ , and  $-2$  (see Figure 2). At these values, chains are not fully wrapped around the NP surfaces with  $\langle R_g^2 \rangle$  values smaller than the plateau values.

When the  $\langle R_g^2 \rangle$  value of a single fully charged chain which is about  $4200$   $\text{\AA}^2$  (data not shown here) is compared, the presence of one NP in the simulation box widely limits  $\langle R_g^2 \rangle$  evolution by fully complexing highly charged PE chains when  $\sigma = 50, 75$ , and  $100$  [ $mC/m^2$ ]. Furthermore, the chain dimension begins to increase at lower  $pH - pK_0$  for higher  $\sigma$  values confirming the important influence of the NP on the PE conformation. In natural processes, flexible histone tails play an important role in gene delivery by regulating chromatin structure. It was found by computer simulations and experimentally<sup>64,65</sup> that the

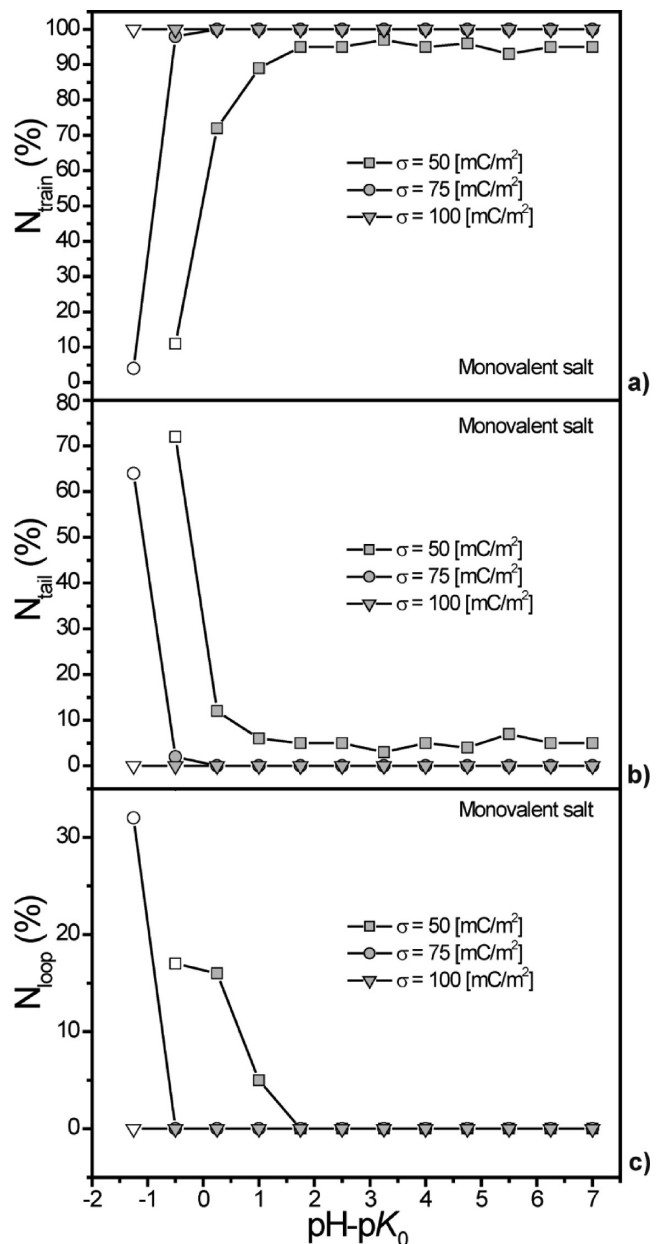


**Figure 4.** Monomer number in (a) trains, (b) tails, and (c) loops as a function of  $pH - pK_0$  for NP charge densities  $\sigma$  equal to  $50, 75$ , and  $100$  [ $mC/m^2$ ]. The lowest  $pH - pK_0$  values of the adsorption domain are represented by open symbols. PE conformations change from desorbed at low  $pH - pK_0$  to fully adsorbed at high  $pH - pK_0$ . Transition to the adsorbed state is sharper considering higher  $\sigma$  values. For  $\sigma = 50$  and  $75$  [ $mC/m^2$ ], a rapid monomer decrease in trains occurs prior the PE desorption leading to an increase of monomers in tails and loops. At  $\sigma = 100$ , PE-NP interactions are so strong that monomers are adsorbed as soon as they are deprotonated leading to instantaneous adsorption.

increase of monovalent salt concentration at low salt concentration leads to the extension of histone tails resulting in the increase of the particle radii of gyration. In our case, we do not vary salt concentration, but PE electrostatic screening is adapted by NP charge density variations. As PE-NP and PE-salt cations attractive interactions are in competition, chain screening by salt becomes softer with the  $\sigma$  increase resulting in the formation of more compact complexes.

Concerning the NP surface charge density of  $25 \text{ [mC/m}^2]$ , a different behavior is observed since no plateau value is reached with the increase of  $\text{pH} - \text{p}K_0$  and the chain dimension increases more or less regularly within the range of  $\text{pH} - \text{p}K_0 = [-2.75; 7]$ . For this  $\sigma$  value,  $(\text{pH} - \text{p}K_0)_{\text{crit}}$  is fixed to 1.75, but the whole monomers are never completely adsorbed even when  $\alpha = 1$  (see Table 1,  $\text{pH} - \text{p}K_0 = [1.75; 6.25]$ ). As the PE chains keep movement liberties,  $\langle R_g^2 \rangle$  continues to increase due to stronger intramolecular interactions. In our study,  $\sigma = 25 \text{ [mC/m}^2]$  then represents a particular situation which will not be taken into account to study the evolution of monomers in trains, tails, and loops in Figure 4 since monomers switch all the time between adsorption and desorption domains.

**Monomer Distribution in Trains, Tails, and Loops.** Figure 4 represents the variation of the monomer number in trains ( $N_{\text{train}}$ ), tails ( $N_{\text{tail}}$ ), and loops ( $N_{\text{loop}}$ ) around the NP as a function of  $\text{pH} - \text{p}K_0$  for NP charge densities equal to 50, 75, and  $100 \text{ [mC/m}^2]$ . Open symbols show the lowest  $\text{pH} - \text{p}K_0$  values of the adsorption domain for each  $\sigma$ . For the highest NP charge density, attractive interactions between charged monomers and the NP are so strong that the PEs are fully adsorbed within the NP first layer as soon as the chains are forming complexes. This feature is revealed in Figure 4a where 100% of monomers are situated in trains when  $\sigma = 100 \text{ [mC/m}^2]$ . With the decrease of the NP surface charge density, most of the monomers are not attracted within the NP first layer at the lowest  $\text{pH} - \text{p}K_0$  values of the adsorption domain. When  $\sigma = 50$  and  $75 \text{ [mC/m}^2]$ , the majority of monomers are first situated in tails, second in loops, and finally in trains. Increasing the PE chain degree of ionization allows a sharp increase of the amount of monomers adsorbed within the NP first layer to be observe. Concerning  $\sigma$  values of 50 and  $75 \text{ [mC/m}^2]$ , it has to be noted that the number of monomers in tails and loops is rapidly increasing with the decrease of the monomers in trains prior to PE desorption. The conformational change from completely desorbed to fully adsorbed is also found sharp when  $\sigma = 75 \text{ [mC/m}^2]$  confirming the rapid complex formation with higher NP surface charge densities.

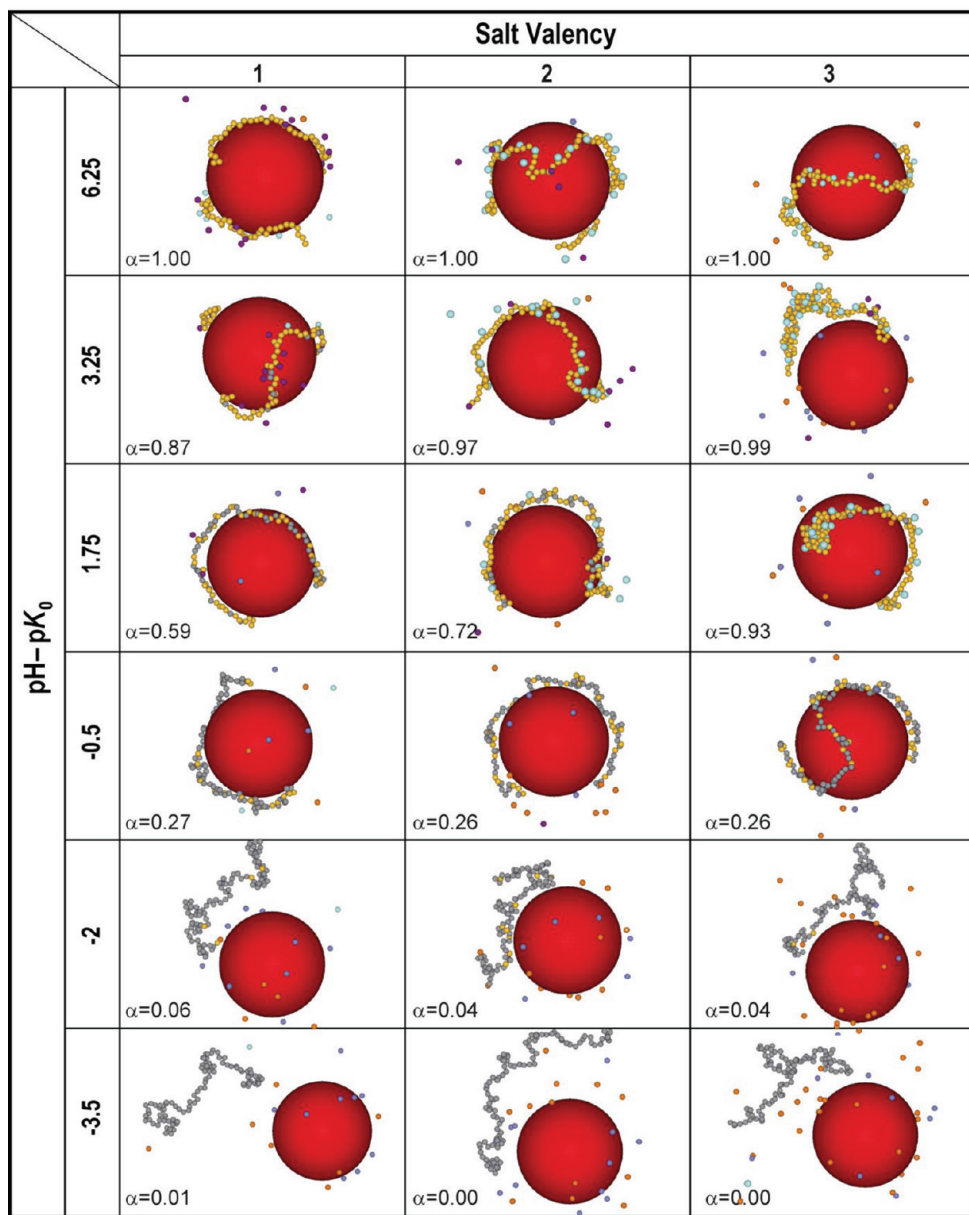
**3.2. Effect of Salt Valency.** We investigate here the case of an isolated weak flexible PE chain (100 monomers) and a NP ( $\sigma = 50 \text{ [mC/m}^2]$ ) surrounded by explicit monovalent counterions as well as mono-, di or trivalent salt particles ( $C_i = 1 \times 10^{-3} \text{ M}$ ). It was shown by SANS experiments<sup>15,66</sup> that a monovalent salt increase on one hand does not influence significantly the primary structure of PE–lysozyme complexes but, on the other hand, enables the fusion of several complexes into larger ones or prevents the cluster formation when short PSS or rodlike Hyaluronan chains are considered. Thus, the influence of salt valency and pH variation on the adsorption of PE chains on NPs and indirectly on the complex primary structure is specifically studied. Table 2 represents the equilibrated conformations of one PE and one NP at various  $\text{pH} - \text{p}K_0$  values and salt valencies. Globally, PE degree of ionization  $\alpha$  increases with  $\text{pH} - \text{p}K_0$  in presence of mono, di and trivalent salt cations hence promoting the PE–NP complex formation. Increasing salt valencies allows to observe higher ionization degrees  $\alpha$  for a given  $\text{pH} - \text{p}K_0$  value due to stronger specific monomer–salt cations associations and screening efficiency. Thus, PE–NP complexation is in direct competition with the association of salt cations around PE backbones. At low  $\text{pH} - \text{p}K_0$ , PE chains are uncharged and NP counterions (blue) as well as monovalent salt anions (orange) are attracted by the nanoparticle due to their negative

charges. Similar behaviors are observed considering mono and divalent salt. With the increase of  $\text{pH} - \text{p}K_0$ , and as long as  $\alpha < 0.5$ , the adsorbed NP counterions and salt anions are progressively released into the bulk and replaced by the charged monomers of the PE. When  $\alpha > 0.5$ , PE chain charge overcompensates the NP charge and chain counterions (purple) as well as salt cations (cyan) are significantly attracted around the chain to compensate the excess of charge of the complex. With monovalent salt, PE counterions and salt cations are indistinguishable, the association is then unspecific. The case with divalent salt results in a specific association of the salt cations with the PE due to stronger monomer–salt attractive interactions. For both salt valencies, i.e., mono and di, PE chains are adsorbed around the NPs when PEs are fully charged. The main difference remains in the adsorbed PE conformations which are more regular (tennis ball) with monovalent salt. Considering divalent salt, no characteristic PE structures are observed demonstrating more labile attractive PE–NP interactions due to stronger attractive PE and repulsive NP interactions with the salt cations.

Considering trivalent salt, the attraction of NP counterions and monovalent salt anions by the NP already occurs at low  $\text{pH} - \text{p}K_0$  values. The adsorption of the trivalent cations around the PE chains when  $\alpha > 0.5$  widely influences the final conformations of NP–PE complexes. Indeed, a subtle competition between PE–NP and PE–salt cations attractive interactions leads to the formation of locally collapse PE segments which are desorbed from the NP surface (for instance  $\text{pH} - \text{p}K_0 = 3.25$  and  $z_i = 3$ ). Thus, the amount of adsorbed PE monomers is reduced with trivalent salt and a few NP counterions and monovalent salt anions remain adsorbed around the NP even at high  $\text{pH} - \text{p}K_0$  values.

**Titration Curves.** PE titration curves in the presence of the NP are presented in Figure 5a and the corresponding  $\Delta pK$  variations in Figure 5b for mono-, di-, and trivalent salt at a concentration of  $1 \times 10^{-3} \text{ M}$ . The NP surface charge density is fixed to  $50 \text{ [mC/m}^2]$ . Titration curves for isolated PE chains surrounded by monovalent salt as well as isolated monomers are also given for comparison. The increase of salt valency significantly modifies the subtle competition between attractive PE–NP and PE–salt cation electrostatic interactions. Different behaviors can be observed above and below the intersecting point with the ideal curve. Indeed, the influence of salt valency is very limited at low  $\text{pH} - \text{p}K_0$  values due to very weak monomer–salt cation associations. Consequently, titration curves for mono, di and trivalent salt are almost identical below the intersecting point with the ideal curve and the corresponding  $\Delta pK$  variations remain negative due to the nanoparticle presence. In that case, the monomer deprotonation is essentially driven by the presence of the positively charged NP. It can be noted that  $\Delta pK$  variations are slightly less important with di and trivalent salt since more salt anion particles are present in the simulation box and consequently attracted by the NP hence reducing the electrostatic effects of the nanoparticle on the chain dissociation degree.

When  $\Delta pK > 0$ , repulsive monomer–monomer interactions are no more counterbalanced by attractive monomer–NP interactions and  $\Delta pK$  regularly increases with the chain degree of ionization for the various salt valencies but remains situated below the isolated chain curve. Also the slope of  $\Delta pK$  curves decreases with the increase of salt valency due to stronger monomer–salt cation associations. Indeed, both salt cations and PE counterions are attracted in the vicinity of the polyelectrolytes

Table 2. Equilibrated Conformations of a Weak Flexible PE Chain and One NP ( $\sigma = 50 \text{ [mC/m}^2\text{]}$ )<sup>a</sup>

<sup>a</sup> Each monomer can be neutral (grey sphere) or carry one negative charge (yellow sphere). Chain and NP monovalent counterions are purple and blue. Cases with mono-, di-, and trivalent salt (cyan spheres) are considered. The PE adsorption is promoted by the increase of the chain linear charge density. When  $\alpha > 0.5$ , the association between monomers and salt cations occurs more strongly with higher salt valencies hence promoting the chain deprotonation and the competition with the PE–NP complexation. When  $z_i = 1$  and 2, and at high  $\text{pH} - pK_0$  values, the adsorbed PE chains are fully wrapped around the NP surface with more regularity with  $z_i = 1$  (tennis ball conformations). Considering  $z_i = 3$ , locally collapsed PE segments around trivalent cations are desorbed confirming the reduced PE–NP complexation.

when  $\Delta pK > 0$  promoting the chain deprotonation process. As a result, the affinity of salt cations with PE chains increases with salt valency leading to titration curves situated closer to the ideal curve and thus lower  $\Delta pK$  values.

**Adsorption/Desorption Limits.** Adsorption/desorption limits of a PE chain at the NP surface in presence of explicit mono, di and trivalent salt are now investigated in Figure 6 by representing  $(\text{pH} - pK_0)_{\text{crit}}$  as a function of various NP surface charge densities  $\sigma = 25, 35, 50, 75$ , and  $100 \text{ [mC/m}^2\text{]}$ .  $(\text{pH} - pK_0)_{\text{crit}}$  decreases with the increase of the NP charge density and larger

PE adsorption domains are observed when  $\sigma$  increases. Considering monovalent salt, the slope of the curve regularly decreases until  $\sigma = 75 \text{ [mC/m}^2\text{]}$ . Beyond this point,  $\sigma$  variations have no influence on the polyelectrolyte adsorption within the NP first layer. By increasing salt valency, stronger monomer–salt cation associations occur hence promoting the competition between PE–NP and PE–salt cation complexation. As a result, the PE–NP adsorption domain is found reduced and the adsorption/desorption limits obtained at higher  $\text{pH} - pK_0$  values.

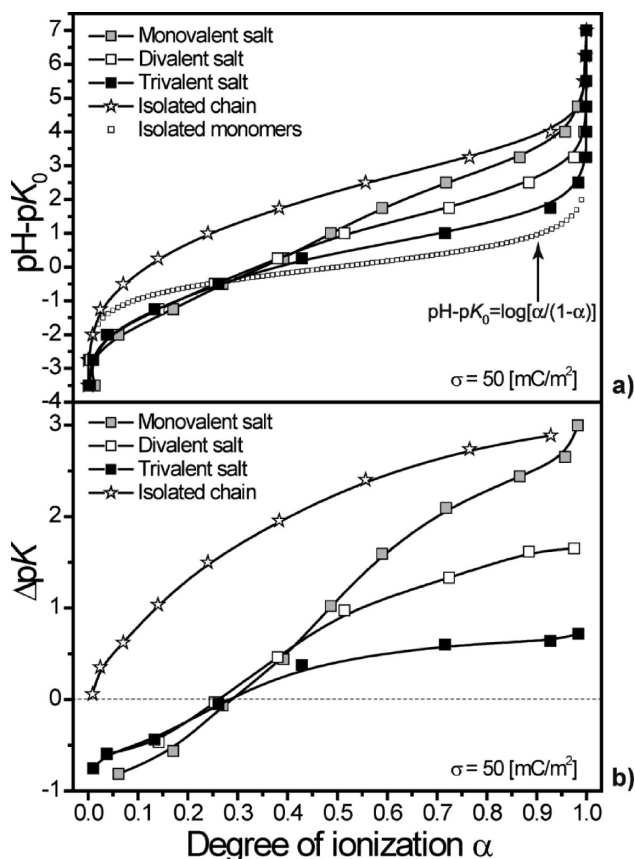


**Figure 5.** (a) Titration curves and (b)  $\Delta pK$  variations of a weak flexible PE chain surrounded by one NP as well as mono-, di-, and trivalent salt. The NP charge density  $\sigma$  is fixed to  $50 \text{ [mC/m}^2\text{]}$ . Below the intersecting point with the ideal curve, salt valency influence is very limited leading to similar titration and  $\Delta pK$  curves. When  $\Delta pK > 0$ , intramolecular monomer–monomer interactions overcompensate PE–NP interactions, and a significant switch is observed between titration and  $\Delta pK$  curves of the various salt valencies. In this domain, chain deprotonation is promoted by higher salt valencies.

The trivalent salt case shows a particular behavior at low  $\sigma$  values since the salt association with monomers is strong enough to prevent the PE chain to complex with the NP due to the formation of PE locally folded segments. Comparing the shape of the curves, an evolution is observed from exponential for monovalent salt to quasi linear for trivalent salt hence showing a modification in the PE adsorption behavior with the variation of salt valency.

**Monomer Distribution in Trains, Tails, and Loops.** The variations of the number of monomers in trains, tails and loops around the NP ( $\sigma = 50 \text{ [mC/m}^2\text{]}$ ) are represented in Figure 7a–c, as a function of  $\text{pH} - \text{p}K_0$  for mono-, di-, and trivalent salt. Star symbols show the lowest  $\text{pH} - \text{p}K_0$  values at which PEs are considered adsorbed. Considering monovalent salt, most of the monomers are situated in tails at lower  $\text{pH} - \text{p}K_0$  values (Figure 7b). Indeed, PE charge density is weak at this value ( $\alpha = 0.27$ ), and only a very limited number of monomers are attracted within the NP first layer hence promoting monomers in tails. The increase of PE–NP attractive interactions with  $\text{pH} - \text{p}K_0$  is followed by a fast increase of monomers in  $N_{\text{train}}$  until  $\text{pH} - \text{p}K_0 = 1.75$ . Beyond this value, the variation of  $\text{pH} - \text{p}K_0$  has little influence on the monomer distribution in which

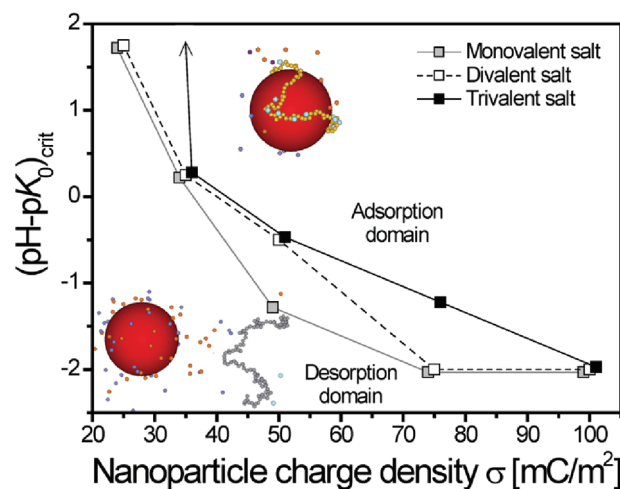


**Figure 6.** Adsorption/desorption limits  $(\text{pH} - \text{p}K_0)_{\text{crit}}$  of a PE chain at the NP surface as a function of the NP charge density  $\sigma$  in presence of monovalent counterions and mono-, di-, and trivalent salt. Larger PE adsorption domains are achieved with the increase of  $\sigma$  due to stronger NP–PE attractive interactions. Higher salt valencies induce the competition between PE–salt cation and PE–NP interactions hence reducing the adsorption domain. At low  $\sigma$  values, trivalent salt cations prevent the complexation of PE and NP due to the formation of locally folded PE segments.

95% remain in trains. Flat conformations are thus achieved when the PE chain is adsorbed.

With divalent salt, a similar behavior is observed, i.e., the increase of the monomer percentage in trains with  $\text{pH} - \text{p}K_0$  values. As already mentioned, the association between monomers and divalent salt cations are stronger and in direct competition with PE–NP attractive interactions. Consequently, PE degree of dissociation has to be higher to observe PE adsorption [Figure 7a,  $\text{pH} - \text{p}K_0 = 0.25$  ( $\alpha = 0.38$ ) for divalent and  $\text{pH} - \text{p}K_0 = -0.5$  ( $\alpha = 0.27$ ) for monovalent salt]. Moreover for a given  $\text{pH} - \text{p}K_0$  value, the number of monomers in trains is smaller before to reach the plateau value demonstrating the impact of the divalent cations on the PE adsorption.

As shown in Figure 7, the further increase of salt valency penalizes more and more the PE adsorption process and a particular behavior is observed with trivalent salt cations. Important fluctuations in the number of monomers in train, tail and loop are observed which are due to the strong association of the monomers with the trivalent cations at the interface between the adsorption layer and solution. Similar trend has already been observed by Lyulin et al.,<sup>67</sup> who studied the role of electrostatic interactions in dendrimer–PE complexes (soft nanoparticles). Although their system is not directly comparable with ours, they observed a significant fraction of monomers which never condense to dendrimer surface already with the presence of divalent cations.

**Radial Distribution Function of Monomers.** The radial distribution functions (RDFs) of monomers around the NP in presence of monovalent and trivalent salt are now calculated for  $\text{pH} - \text{p}K_0$  values of  $-0.5$ ,  $+1$ , and  $+7$  (Figure 8). It has to be noted that PE chains are situated within the adsorption domain for the whole  $\text{pH} - \text{p}K_0$  values and valencies considered here.

Concerning monovalent salt (Figure 8a), the monomer density close to the NP surface increases with  $\text{pH} - \text{p}K_0$  due to the increase of the electrostatic attractive monomer–NP interactions.

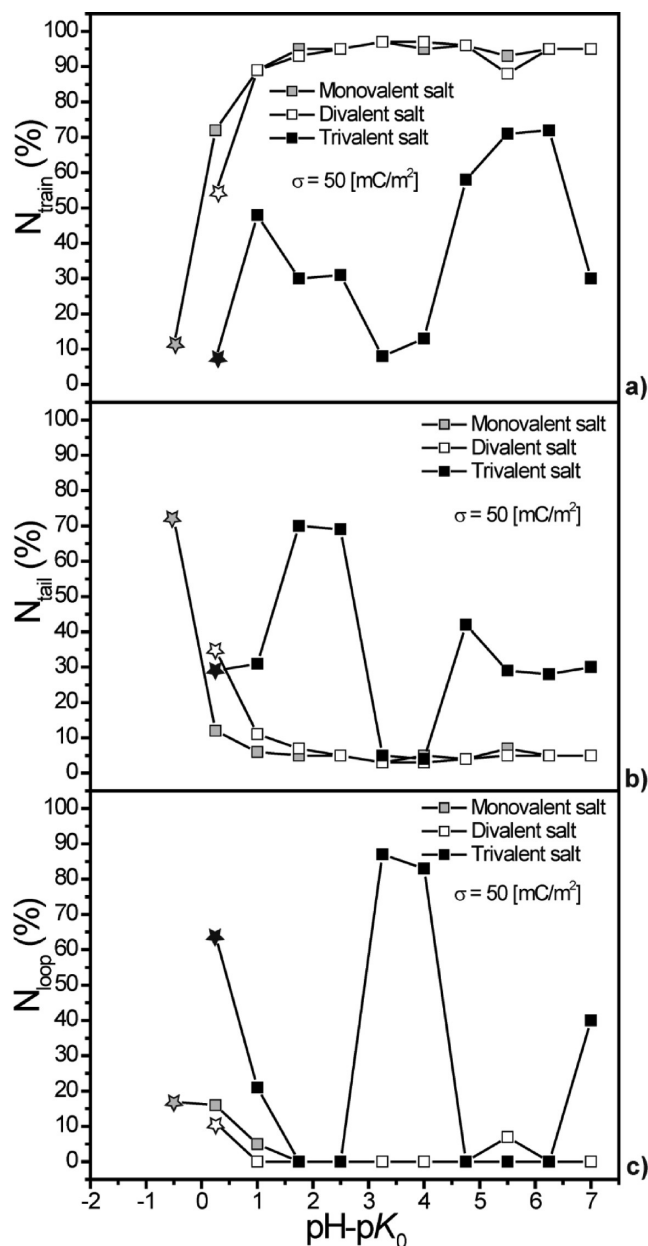


**Figure 7.** Number of monomers in (a) trains, (b) tails, and (c) loops at the NP surface ( $\sigma = 50 \text{ [mC/m}^2\text{]}$ ) as a function of  $pH - pK_0$  with mono-, di-, and trivalent salt. The lowest  $pH - pK_0$  values of the adsorption domain are represented by star symbols. At low  $pH - pK_0$  values, PE chains remain desorbed for the whole salt valencies. Considering mono and divalent salt, a sharp transition to the adsorbed state is observed with the increase of the PE linear charge density until plateau values (panel a). Due to stronger divalent cation association with the chain, the PE degree of ionization  $\alpha$  has to be higher to observe PE adsorption. Constant fluctuations in panels a–c are obtained due to the presence of the trivalent cations in the vicinity of the adsorption layer.

Moreover, the maxima of monomer density are moving closer to the NP surface with the increase of  $pH - pK_0$  values confirming the flat conformations adopted by the PE chains with most of monomers in trains.

The situation involving trivalent cations (Figure 8b) shows a different behavior. By increasing  $pH - pK_0$ , the RDF maxima are shifted to lower values indicating that the PE adsorption is

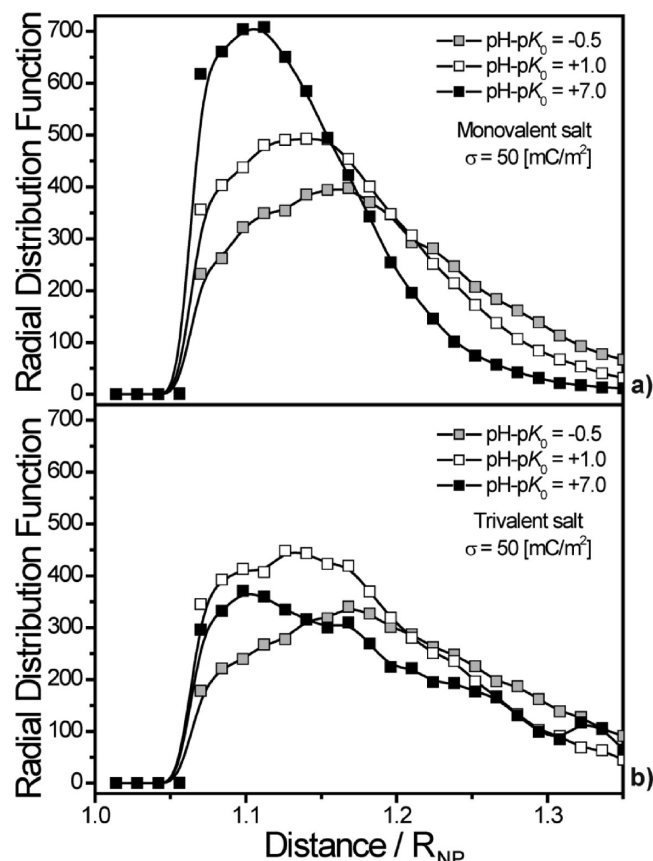


**Figure 8.** Radial distribution functions (RDFs) of PE monomers around the NP surface ( $\sigma = 50 \text{ [mC/m}^2\text{]}$ ) with (a) mono- and (b) trivalent salt. For both salt valencies, the RDF peak values are shifted closer to the NP surface with the increase of the PE linear charge density indicating that the monomer adsorption is promoted. With monovalent salt, the adsorbed PE chain adopts flat conformations with most of monomers in the NP first layer leading to a RDF increase with  $pH - pK_0$ . With trivalent salt, no important RDF increase is achieved confirming a reduced PE–NP affinity due to the effect of trivalent cations.

promoted by increasing the dissociation degree of the chain. However, the monomer density is found relatively large and less important close to the NP surface in comparison to the situation with monovalent salt in agreement with dendrimer–PE studies.<sup>67</sup> This feature results from the strong association of the PE monomers with the trivalent cations, therefore promoting the competition with the PE–NP interactions, which significantly reduces the monomer affinity with the NP surface. Moreover, as shown in Table 2, PE chains adopt locally folded structures in presence of multivalent salt cations. This chain conformational change is of main importance since the compaction of biological complexes such as chromatin can occur with multivalent salt modifying their specific roles.<sup>68</sup> In industrial processes, PE-grafted macroions are widely used and the stabilization or destabilization of such suspensions is essential. Arya<sup>69</sup> showed that the phase separation of such complexes occurs when the PE and macroion charges are comparable and is pH adjustable. Thus, in a destabilized solution, the addition of trivalent salt cations should be followed by the disappearing of phase separation due to the increase of PE degree of ionization and compaction hence favoring the repulsive interactions between colloidal complexes.

## 4. CONCLUSION

MC simulations were carried out to investigate the complexation behavior of one weak flexible PE chain with one NP using a full long-range Coulomb electrostatic potential and an explicit description of counterions and salt particles. We focused on the influence of the variation of pH as well as NP surface charge density and salt valency on the chain protonation/deprotonation process and amount of adsorbed monomers. Conformational properties of the PE chains were also investigated.

We found that the NP presence plays a significant role by modifying acid/base properties of the PE chain. The PE deprotonation process is thus improved by the pH increase as well as by the NP proximity due to attractive electrostatic interactions between the two objects. Within the whole titration range, the NP presence allows to obtain situations at which the intramolecular monomer interactions are exactly counterbalanced by PE–NP attractions leading to ideal deprotonation situations. The PE monomer adsorption within the NP first layer is directly dependent on the interaction strength between the PE and the NP. In this study at low pH –  $pK_0$  ( $\sigma = 25$  [mC/m<sup>2</sup>]), the chain dimension continuously increases with pH –  $pK_0$  due to low monomer attraction by the NP. The PE chain is then adsorbed at high chain degree of ionization via a limited number of monomers. At higher NP charge densities, PE conformations change rapidly from desorbed to fully adsorbed with the increase of pH –  $pK_0$  values leading to chain dimensions which are comparable with the NP size. The increase of the NP charge density thus allows the formation of strong complexes with regular and fully wrapped PE conformations. Moreover, the negative charge excess remaining after the PE–NP complexation is compensated by the condensation of PE counterions and salt cations around the polyelectrolyte chain.

The increase of salt valency allows a stronger association of salt cations with the chain backbone hence resulting in a competition between attractive PE–salt cation and PE–NP electrostatic interactions. The adsorbed PE conformations thus become less regular and more labile leading to locally collapsed segments with trivalent salt in particular when  $\alpha > 0.5$ . The amount of adsorbed monomers does not significantly increase with pH –  $pK_0$  and remains limited in this situation. Comparing with monovalent salt, the PE adsorption domain decreases hence confirming the negative impact of the presence of cations of higher valencies on the PE–NP complexation process.

This paper presents results obtained with a generic model which includes explicitly multivalent ions and leading to similar complex structures to that found in real systems. Due to the specific behavior of multivalent ions, some of the observed effects might not have been explained by Debye–Hückel approximations. The results reported here have been obtained by considering identical monomers types, no intrinsic chain rigidity, low salt concentration values, etc. The model, however, is not restricted to this, and instead of considering a homogeneous surface charge distribution, one could consider discrete charge distribution of titrable sites at the nanoparticle surface. This would allow to observe other specific effects resulting from correlations between surface inhomogeneities, charged monomers and charged salt particles.

## AUTHOR INFORMATION

### Corresponding Author

\*E-mail: serge.stoll@unige.ch.

## ACKNOWLEDGMENT

The authors are grateful to S. Le Faucheur, D. Palomino, M. Seijo, and S. Ulrich for their encouragements and stimulating discussions. We also gratefully acknowledge the financial support received from the following sources: Département de l'Instruction Publique de l'Etat de Genève and Swiss National Foundation (project 200021\_135240).

## REFERENCES

- (1) Ullner, M. *Handb. Polyelectrolytes Their Appl.* **2002**, *3*, 271–308.
- (2) Wandrey, C.; Hunkeler, D. *Handb. Polyelectrolytes Their Appl.* **2002**, *2*, 147–172.
- (3) Cooper, C. L.; Dubin, P. L.; Kayitmazer, A. B.; Turksen, S. *Curr. Opin. Colloid Interface Sci.* **2005**, *10*, 52–78.
- (4) de Vries, R.; Cohen Stuart, M. *Curr. Opin. Colloid Interface Sci.* **2006**, *11*, 295–301.
- (5) Ulrich, S.; Seijo, M.; Stoll, S. *Curr. Opin. Colloid Interface Sci.* **2006**, *11*, 268–272.
- (6) Dobrynin, A. V. *Curr. Opin. Colloid Interface Sci.* **2008**, *13*, 376–388.
- (7) Schwoyer, W. L. K. *Polyelectrolytes for Water and Wastewater Treatment*; CRC press: Boca Raton, FL, 1981.
- (8) Allen, T. M.; Cullis, P. R. *Science* **2004**, *303*, 1818–1822.
- (9) Berret, J.-F.; Schonbeck, N.; Gazeau, F.; El Kharrat, D.; Sandre, O.; Vacher, A.; Airiau, M. *J. Am. Chem. Soc.* **2006**, *128*, 1755–1761.
- (10) Rasteiro, M. G.; Garcia, F. A. P.; Ferreira, P. J.; Antunes, E.; Hunkeler, D.; Wandrey, C. *J. Appl. Polym. Sci.* **2010**, *116*, 3603–3612.
- (11) Wang, H.; Roman, M. *Biomacromolecules* **2011**, *12*, 1585–1593.
- (12) Jeon, J.; Dobrynin, A. V. *J. Phys. Chem. B* **2006**, *110*, 24652–24665.
- (13) Larin, S. V.; Darinskii, A. A.; Lyulin, A. V.; Lyulin, S. V. *J. Phys. Chem. B* **2010**, *114*, 2910–2919.
- (14) Dias, R. S.; Pais, A. A. C. C.; Linse, P.; Miguel, M. G.; Lindman, B. *J. Phys. Chem. B* **2005**, *109*, 11781–11788.
- (15) Cousin, F.; Gummel, J.; Clemens, D.; Grillo, I.; Boué, F. *Langmuir* **2010**, *26*, 7078–7085.
- (16) Dobrynin, A. V.; Rubinstein, M. *Prog. Polym. Sci.* **2005**, *30*, 1049–1118.
- (17) Mandel, M. *Eur. Polym. J.* **1970**, *6*, 807–22.
- (18) Onufriev, A.; Case, D. A.; Ullmann, G. M. *Biochemistry* **2001**, *40*, 3413–3419.
- (19) Ullmann, G. M. *J. Phys. Chem. B* **2003**, *107*, 1263–1271.
- (20) Ullner, M.; Jönsson, B.; Söderberg, B.; Peterson, C. *J. Chem. Phys.* **1996**, *104*, 3048–57.
- (21) Panagiotopoulos, A. Z. *J. Phys.: Condens. Matter* **2009**, *21*, 424113.
- (22) Kayitmazer, A. B.; Seyrek, E.; Dubin, P. L.; Staggemeier, B. A. *J. Phys. Chem. B* **2003**, *107*, 8158–8165.
- (23) Zhang, H.; Dubin, P. L.; Ray, J.; Manning, G. S.; Moorefield, C. N.; Newkome, G. R. *J. Phys. Chem. B* **1999**, *103*, 2347–2354.
- (24) McQuigg, D. W.; Kaplan, J. I.; Dubin, P. L. *J. Phys. Chem.* **1992**, *96*, 1973–1978.
- (25) Berret, J.-F.; Yokota, K.; Morvan, M. *Soft Mater.* **2004**, *2*, 71.
- (26) Sehgal, A.; Lalatonne, Y.; Berret, J.-F.; Morvan, M. *Langmuir* **2005**, *21*, 9359–9364.
- (27) Berret, J.-F. *Colloid Polym. Sci.* **2009**, *287*, 801–810.
- (28) Koupanou, E.; Ahualli, S.; Glatter, O.; Delgado, A.; Krumeich, F.; Leonidis, E. *Langmuir* **2010**, *26*, 16909–16920.
- (29) Messina, R. *J. Phys.: Condens. Matter* **2009**, *21*, 113102.
- (30) Dias, R. S.; Pais, A. A. C. C. *Adv. Colloid Interface Sci.* **2010**, *158*, 48–62.
- (31) Netz, R. R.; Joanny, J.-F. *Macromolecules* **1999**, *32*, 9026–9040.
- (32) Boroudjerdi, H.; Kim, Y.-W.; Naji, A.; Netz, R. R.; Schlagberger, X.; Serr, A. *Phys. Rep.* **2005**, *416*, 129–199.
- (33) Schiessel, H. *J. Phys.: Condens. Matter* **2003**, *15*, R699–R774.
- (34) Schiessel, H. *Macromolecules* **2003**, *36*, 3424–3431.

- (35) Manning, G. S. *J. Phys. Chem. B* **2003**, *107*, 11485–11490.
- (36) Winkler, R. G.; Cherstvy, A. G. *J. Phys. Chem. B* **2007**, *111*, 8486–8493.
- (37) Nguyen, T. T.; Shklovskii, B. I. *J. Chem. Phys.* **2001**, *114*, 5905.
- (38) Montes, S.; Grande, H.; Etxeberria, A.; Pomposo, J. A. *J. Nano Res.* **2009**, *6*, 123–132.
- (39) Wallin, T.; Linse, P. *Langmuir* **1996**, *12*, 305–14.
- (40) Jonsson, M.; Linse, P. *J. Chem. Phys.* **2001**, *115*, 10975.
- (41) Akinchina, A.; Linse, P. *Macromolecules* **2002**, *35*, 5183–5193.
- (42) Stoll, S.; Chodanowski, P. *Macromolecules* **2002**, *35*, 9556–9562.
- (43) Wallin, T.; Linse, P. *J. Phys. Chem. B* **1997**, *101*, 5506–5513.
- (44) Chodanowski, P.; Stoll, S. *J. Chem. Phys.* **2001**, *115*, 4951.
- (45) Carlsson, F.; Linse, P.; Malmsten, M. *J. Phys. Chem. B* **2001**, *105*, 9040–9049.
- (46) da Silva, F. L. B.; Jönsson, B. *Soft Matter* **2009**, *5*, 2862.
- (47) de Carvalho, S. J. *Europhys. Lett.* **2010**, *92*, 18001.
- (48) Hu, Y.; Ni, R.; Cao, D.; Wang, W. *Langmuir* **2008**, *24*, 10138–10144.
- (49) Ullner, M.; Jönsson, B. *Macromolecules* **1996**, *29*, 6645–6655.
- (50) Ullner, M.; Woodward, C. E. *Macromolecules* **2000**, *33*, 7144–7156.
- (51) Laguecir, A.; Ulrich, S.; Labille, J.; Fatin-Rouge, N.; Stoll, S.; Buffle, J. *Eur. Polym. J.* **2006**, *42*, 1135–1144.
- (52) Ulrich, S.; Laguecir, A.; Stoll, S. *Macromolecules* **2005**, *38*, 8939–8949.
- (53) Ulrich, S.; Seijo, M.; Laguecir, A.; Stoll, S. *J. Phys. Chem. B* **2006**, *110*, 20954–20964.
- (54) Klos, J.; Pakula, T. *J. Chem. Phys.* **2005**, *123*, 024903/1–024903/8.
- (55) Hsiao, P.-Y.; Luijten, E. *Phys. Rev. Lett.* **2006**, *97*, 148301/1–148301/4.
- (56) Carnal, F.; Stoll, S. *J. Chem. Phys.* **2011**, *134*, 044909.
- (57) Tian, W.-d.; Ma, Y.-q. *J. Phys. Chem. B* **2009**, *113*, 13161–13170.
- (58) Metropolis, N.; Rosenbluth, A. W.; Rosenbluth, M. N.; Teller, A. H.; Teller, E. *J. Chem. Phys.* **1953**, *21*, 1087–92.
- (59) Manning, G. S. *J. Chem. Phys.* **1969**, *51*, 924–33.
- (60) Reed, C. E.; Reed, W. F. *J. Chem. Phys.* **1992**, *96*, 1609–20.
- (61) Ullner, M.; Jönsson, B.; Widmark, P. O. *J. Chem. Phys.* **1994**, *100*, 3365–6.
- (62) Khrapunov, S. N.; Dragan, A. I.; Sivolob, A. V.; Zagariya, A. M. *Biochim. Biophys. Acta, Gene Struct. Expression* **1997**, *1351*, 213–222.
- (63) Carnal, F.; Ulrich, S.; Stoll, S. *Macromolecules* **2010**, *43*, 2544–2553.
- (64) Bertin, A.; Leforestier, A.; Durand, D.; Livolant, F. *Biochemistry* **2004**, *43*, 4773–4780.
- (65) Arya, G.; Zhang, Q.; Schlick, T. *Biophys. J.* **2006**, *91*, 133–150.
- (66) Morfin, I.; Buhler, E.; Cousin, F.; Grillo, I.; Boué, F. *Biomacromolecules* **2011**, *12*, 859–870.
- (67) Lyulin, S. V.; Vattulainen, I.; Gurtovenko, A. A. *Macromolecules* **2008**, *41*, 4961–4968.
- (68) Arya, G.; Schlick, T. *J. Phys. Chem. A* **2009**, *113*, 4045–4059.
- (69) Arya, G. *J. Phys. Chem. B* **2009**, *113*, 15760–15770.